Effect of cross-field flow on inertial Alfvén waves of small transverse scale

T. Drozdenko and G. J. Morales
Department of Physics and Astronomy, University of California at Los Angeles, Los Angeles, California 90095

(Received 4 December 2000; accepted 27 March 2001)

This analytic study examines the effect of cross-field flow on a microscopic current channel. To illustrate the subtle interplay between finite electron inertia and flows, a simple model of excitation of a microscopic current channel is considered. The model consists of a slab antenna exciter with a transverse width on the order of the electron skin-depth driven at a single frequency. The antenna is fixed in the laboratory frame and embedded within a plasma that has a uniform drift across the confining magnetic field. The combined effects of the plasma flow and the intrinsic, collisionless, cross-field expansion of the current channel lead to standing wave structures across the confining magnetic field. The resulting parallel electric fields generate an array of current filaments of alternating polarity which individually have transverse width smaller than the original channel. These results may help interpret laboratory and spacecraft measurements of Alfvénic turbulence and could lead to the development of a diagnostic tool to map plasma flows. © *2001 American Institute of Physics.* [DOI: 10.1063/1.1374587]

I. INTRODUCTION

The interaction of large-scale, quasi-static flows across the confining magnetic field with microscopic plasma turbulence is a topic of considerable interest to the controlled magnetic fusion community[1–4] as well as to space plasma researchers.[5–11] While these two separate (but closely related) disciplines agree on the importance of this topic, at the present time, the prevailing perspectives within each area seem somewhat contradictory. It is broadly perceived by the fusion investigators that the high degree of symmetrization imparted by large-scale flows leads to a significant taming of microscopic turbulence whose very beneficial outcome is the enhanced confinement of the plasma, e.g., H-modes.[12,13] The space researchers view the large-scale flows as sources that lead to the development of microscopic structures in naturally occurring plasmas with the outcome being spectacular particle acceleration events, e.g., the aurora borealis. There exists ample observational evidence to substantiate both perspectives, thus it is clear that the role of cross-field flows on microscopic structures is a subtle topic that deserves detailed theoretical and laboratory studies.

The present analytic study focuses on a narrow but generic aspect of this difficult problem. The issue considered is the response of a microscopic current channel to an imposed cross-field flow. By microscopic, it is meant that the original transverse scale of the current channel is on the order of the electron skin-depth c/ω_{pe}, where c is the speed of light and ω_{pe} is the electron plasma frequency. At these small transverse scales, the evolution of current channels is regulated by the parallel electric fields associated with shear Alfvén waves. To elucidate the nontrivial linear effects associated with the flow, we consider the simplest model of excitation for such a structure, namely a slab antenna exciter fixed in the laboratory frame and driven at a single frequency ω. Of course, the general situation of pulse excitation of narrow current channels, as may result spontaneously in a plasma, must be constructed from an understanding of the single-frequency behavior.

The physics of the situation considered consists of the interplay between the forcing effect of the flow and the inertia of the electrons, which respond swiftly to the induced parallel electric fields. When electron inertia is neglected, as is typical of the ideal magnetohydrodynamic (MHD) studies, the predicted behavior is that the current channel is freely convected without distortion by the flow. However, in the absence of flow finite electron inertia introduces an intrinsic expansion by a cone angle[14,15] given by $\tan\theta_c=(\omega/\Omega_i)\times(m/M)^{1/2}$ where Ω_i is the ion cyclotron frequency, m refers to the electron mass, and M refers to the ion mass. It is found in the present study that the combined effect of the flow and the collisionless cross-field expansion (i.e., skin-depth) gives rise to standing wave structures across the confining magnetic field. These standing wave structures in turn cause initially top-hat current profiles to evolve into an array of microscopic current channels of much smaller spatial extent, but whose overall width exceeds the original width of the channel.

Aside from the interest in relating these results to transport and structure formation problems, the effect considered here is useful in providing insight into aspects of Alfvénic turbulence (i.e., the cross-field flow could be viewed as a large scale Alfvén wave) and may be valuable in developing a basic laboratory diagnostic that maps unknown plasma flows.

It should be mentioned that in certain situations encountered in laboratory and space applications, nonuniform cross-field flows can be present and can lead to other important effects that are not considered in this study.

The manuscript is organized as follows. Section II outlines the topological changes caused by a cross-field flow on the propagation characteristics of shear Alfvén waves in the

inertial regime. A simple model describing the excitation of a shear Alfvén wave by axial current modulation is presented in Sec. III. The salient features of the spatial structure of the shear wave and associated current channel are shown in Sec. IV. Conclusions are given in Sec. V.

II. PROPAGATION CHARACTERISTICS

In this section, we assess the changes produced by a uniform, time-independent, cross-field flow on the propagation characteristics of a shear Alfvén wave in the inertial regime, i.e., under plasma conditions such that the electron plasma beta satisfies the condition $\beta_e \ll m/M$. Thus, the behavior of the ions and electrons is well described by the cold plasma fluid equations.

In the linear regime investigated in this section, all the physical quantities (electric field $\mathbf{E}'$, magnetic field $\mathbf{B}'$, velocity $\mathbf{v}'_\alpha$, current $\mathbf{j}'_\alpha$) have space–time $(\mathbf{r},t)$ functional dependence of the form

$$F' = F e^{i(\mathbf{k}\cdot\mathbf{r}-\omega t)} + \text{c.c.}, \tag{1}$$

where the primed quantity F' is the physical variable and the unprimed one F corresponds to the complex amplitude.

With this convention, the linearized equation of motion for species α having charge q_α and mass m_α takes the form

$$-im_\alpha(\omega-\mathbf{k}\cdot\mathbf{v}_D)\mathbf{v}_\alpha = q_\alpha\mathbf{E} + \frac{q_\alpha}{c}(\mathbf{v}_\alpha\times B_0) + \frac{q_\alpha}{c}(\mathbf{v}_D\times\mathbf{B}), \tag{2}$$

where $\mathbf{B}_0$ is the static confining magnetic field and $\mathbf{v}_D$ is the cross-field flow velocity.

As is appropriate for the description of shear Alfvén waves in the regime $\omega \ll \Omega_i$, the axial component of the wave field, $B_\parallel$, is negligible and the currents supporting the mode consist of the parallel electron current and the transverse ion current (due to the polarization drift proportional to M).

Using Faraday's law to eliminate the transverse component of the wave magnetic field in terms of the components of the wave electric field $(E_\parallel, E_\perp)$ results in the electron current

$$j_\parallel = i\frac{n_0 e^2}{m\omega}\left[E_\parallel + \frac{k_\parallel v_D}{(\omega-k_\perp v_D)}E_\perp\right], \tag{3}$$

and the ion current

$$j_\perp = -i\frac{n_0 M c^2}{B_0^2}\omega E_\perp, \tag{4}$$

where the perpendicular notation refers to the direction of the flow velocity $\mathbf{v}_D$ having magnitude v_D. In Eq. (4) the convective current resulting from the product of the density fluctuation and v_D is not included because it can be shown by using Poisson's equation that it gives rise to very small corrections for the problem considered.

It should be mentioned that the apparent singularity at $\omega = k_\perp v_D$ in Eq. (3) is automatically removed when the self-consistent electric fields are evaluated in the presence of the flow. It is also useful to recognize that the term responsible for the collisionless skin-effect (proportional to $E_\parallel$) does not experience a modification due to the flow, thus the electrons continue to provide the usual inertial/shielding effect. For electrons, the combined effect of the Doppler shift and the magnetic force proportional to $\mathbf{v}_D\times\mathbf{B}$ cancel each other and leaves the skin effect unchanged.

Using Ampere's law with the displacement current neglected, as is appropriate for shear Alfvén waves, yields the dispersion relation

$$\omega - k_\perp v_D = \frac{k_\parallel v_A}{\sqrt{1+k_\perp^2\delta^2}}, \tag{5}$$

where $v_A = B_0/(4\pi n_0 M)^{1/2}$ is the Alfvén speed and $\delta = c/\omega_{pe}$.

This simple result contains the key ingredients necessary to understand how a current channel is convected by a cross-field flow, but the actual structure of the resulting spatial pattern does not become evident until the behavior of a realistic $k_\perp$ spectrum is considered, as is shown in Sec. IV. The essence of Eq. (5) is that the wave frequency undergoes the usual Doppler shift associated with motion, but the topology associated with the electron skin-depth is unaltered.

The components of the group velocity associated with Eq. (3) are

$$(v_g)_\parallel = \frac{\partial\omega}{\partial k_\parallel} = \frac{v_A}{\sqrt{1+k_\perp^2\delta^2}}, \tag{6}$$

$$(v_g)_\perp = \frac{\partial\omega}{\partial k_\perp} = v_D - \frac{v_A k_\parallel k_\perp \delta^2}{(1+k_\perp^2\delta^2)^{3/2}}. \tag{7}$$

Accordingly, the propagation angle θ_g for Alfvénic disturbances in the presence of flow is given by

$$\tan\theta_g = \frac{(v_g)_\perp}{(v_g)_\parallel} = \frac{v_D(1+2k_\perp^2\delta^2)-\omega k_\perp\delta^2}{v_A\sqrt{1+k_\perp^2\delta^2}}. \tag{8}$$

In the absence of flow $(v_D = 0)$, the propagation angle is

$$\tan\theta_g \to -\frac{\omega k_\perp\delta^2}{v_A\sqrt{1+k_\perp^2\delta^2}}, \tag{9}$$

in which the negative sign indicates that, in the transverse direction, the inertial shear Alfvén wave is a backward wave. In the limit of small transverse scales (i.e., $k_\perp\delta \gg 1$) the propagation becomes independent of $k_\perp$ and results in the cone angle

$$\tan\theta_c = \frac{\omega}{\Omega_i}\sqrt{\frac{m}{M}}, \tag{10}$$

whose effect is to provide a bounding angle for the expansion of current channels in the absence of flows.

The dependence of the tangent of the propagation angle (scaled to $\tan\theta_c$) on the scaled perpendicular wave number $k_\perp\delta$ is shown in Fig. 1 for different values of the scaled flow velocity $U = v_D/(\omega\delta)$. In the absence of flow $(U=0)$ it is seen that the spectral components with $k_\perp < 0$ propagate along $\theta_g > 0$ while those with $k_\perp > 0$ corresponds to propagation along $\theta_g < 0$, as is expected of a backward wave. For small, positive flow $(U=0.1)$ it is found that the region with

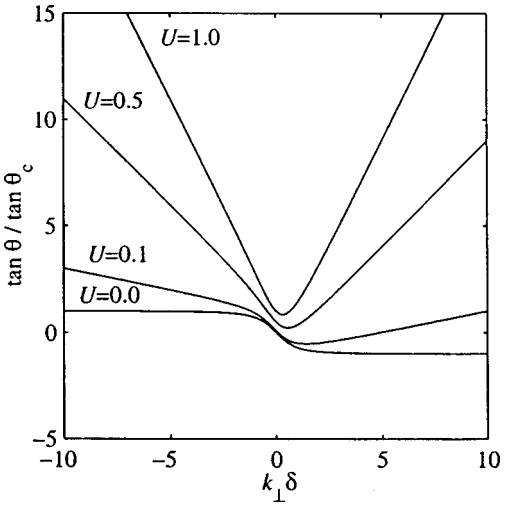

FIG. 1. Dependence of tangent of the propagation angle (scaled to the tangent of the cone angle) on scaled perpendicular wave number for different values of the scaled flow velocity $U=v_D/(\omega\delta)$, where $\delta=c/\omega_{pe}$.

$k_\perp>0$ exhibits a reversal in the propagation direction. The larger $k_\perp$ values start to propagate in the direction of the flow, but there is a region of small $k_\perp>0$ that still propagates against the flow. Beyond a critical value of the drift velocity, however, all the spectral components with $k_\perp>0$ are convected with the flow. For larger values of U, it is seen from Fig. 1 that at a fixed angle of propagation the pattern consists of positive and negative $k_\perp$ components, but having nearly identical magnitude, thus suggesting the natural development of a nearly standing-wave pattern at large flow velocities. In the limit of large drifts, the large $k_\perp$ components of the spectrum propagate along

$$\tan\theta_g \rightarrow 2U|k_\perp|\delta\tan\theta_c, \tag{11}$$

while the small $k_\perp$ components follow the angle predicted by ideal MHD, namely,

$$\tan\theta_g \rightarrow \frac{v_D}{v_A}. \tag{12}$$

III. EXCITATION MODEL

To simplify the calculation and to clearly illustrate the effects produced by a plasma flow, in this study we consider a slab version of the disk modulator used previously[14] to investigate the structure of shear Alfvén waves of small transverse scale. In spite of its simplicity, the theoretical current-modulator model has provided a reasonably accurate description of the excitation properties exhibited by the more elaborate configurations used in laboratory experiments.[16,17]

Figure 2 provides a schematic of the ideal exciter envisioned in this study. It consists of a transparent slab-mesh, placed across the confining magnetic field $\mathbf{B}_0$. The center of the exciter corresponds to the origin of a Cartesian coordinate system (x,y,z) with the z-direction along $\mathbf{B}_0$. The exciter is assumed to be infinite along the x direction, while its width in the y-direction is a. The exciter is assumed to be connected to an external generator operating at frequency ω whose role is to provide an oscillatory surface charge $\sigma(y)$

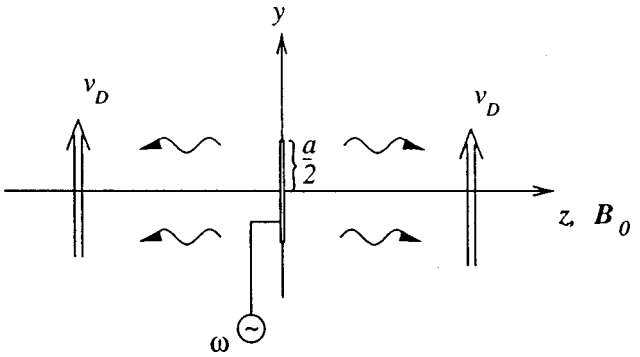

FIG. 2. Schematic of excitation model. A transparent strip exciter of width a (on the order of the electron skin-depth) is modulated by a generator at frequency ω in a plasma with a bulk flow velocity v_D along the positive y direction. The confining magnetic field B_0 is perpendicular to the exciter.

at $z=0$. The self-consistent parallel electric field generated by σ drives oscillatory plasma currents that satisfy the continuity equation at $z=0$,

$$j_{ez}^{+}-j_{ez}^{-}=i\omega\sigma, \tag{13}$$

where j_{ez} refers to the parallel electron current density and the superscripts $(+)$ and $(-)$ refer to the values immediately to the right and left of the exciter, respectively. Of course, the $(+)$ current density is equal in magnitude to the $(-)$ current density but has opposite direction.

Introducing a Fourier transform in the y-direction having the form

$$\sigma(y)=\int_{-\infty}^{+\infty}\frac{dk_\perp}{2\pi}\tilde{\sigma}(k_\perp)e^{ik_\perp y} \tag{14}$$

results in

$$\tilde{\sigma}(k_\perp)=\frac{2\sigma_0\sin(k_\perp a/2)}{k_\perp}, \tag{15}$$

for a uniform charge density of magnitude σ_0. Aside from its simplicity, this model leads to the excitation, at the injection surface, of a uniform current channel of width a.

Using a Fourier transform in the y direction as in Eq. (14) for the current density and applying the symmetry between the $(+)$ and $(-)$ direction results in

$$\tilde{J}_{ez}(k_\perp, z=0^+)=i\frac{\omega\sigma_0\sin(k_\perp a/2)}{k_\perp}. \tag{16}$$

Representing the components of the relevant field quantities F_j' by a generalization of the plane-wave description given by Eq. (1) to incorporate a spectrum of $k_\perp$, as is appropriate to describe the strip-exciter, results in

$$F_j'(y,z,t)=\int_{-\infty}^{+\infty}\frac{dk_\perp}{2\pi}\int_{-\infty}^{+\infty}\frac{dk_\parallel}{2\pi}\tilde{F}_j(k_\perp,k_\parallel,\omega)e^{i(k_\perp y+k_\parallel z-\omega t)} + \text{c.c.} \tag{17}$$

Using the parallel and transverse current densities given by Eqs. (3) and (4) results in the Fourier-transformed, electric field components

$$\tilde{E}_x=0, \tag{18}$$

$$\tilde{E}_y = \frac{4\pi\sigma_0\omega}{c^2} v_A \sqrt{1+k_\perp^2\delta^2} \frac{\sin(k_\perp a/2)}{k_\perp^2}, \tag{19}$$

$$\tilde{E}_\parallel = \frac{4\pi\sigma_0\omega}{c^2} \frac{\sin(k_\perp a/2)}{k_\perp^3} [\omega k_\perp^2 \delta^2 - k_\perp v_D (1+k_\perp^2\delta^2)]. \tag{20}$$

Using Faraday's law, the corresponding magnetic field components are found to be

$$\tilde{B}_y = \tilde{B}_z = 0, \tag{21}$$

$$\tilde{B}_x = -\frac{4\pi\sigma_0\omega \sin(k_\perp a/2)}{c k_\perp^2}. \tag{22}$$

In Eqs. (19), (20), and (22) the relationship between $k_\parallel$ and $k_\perp$ resulting from Eq. (5) has been applied in anticipation of its usage to extract the asymptotic (in the z direction) behavior of the fields, i.e., the inverse Fourier transform is approximated by the dominant response arising from the pole contribution due to the shear Alfvén wave, e.g.,

$$F_j(x,z;\omega) \to \int_{-\infty}^{+\infty} \frac{dk_\perp}{2\pi} e^{k_\perp y} e^{ik_A z\sqrt{1+k_\perp^2\delta^2}(1-k_\perp v_D/\omega)} \tilde{F}_j, \tag{23}$$

where $k_A = \omega/v_A$.

From Eqs. (19)–(23) it is recognized that the useful scaling of the problem corresponds to

$$\rho = \frac{2y}{a}, \quad \xi = k_A z, \tag{24}$$

with the two independent parameters being

$$p = \frac{a\omega_{pe}}{2c} \equiv \frac{a}{2\delta}, \quad U = \frac{2v_D}{\omega a}. \tag{25}$$

Using these scaled quantities, the spatial dependence of the magnetic field is given by

$$B_x(y,z;\omega) = -\frac{\sigma_0\omega a}{c} b(\rho,\xi;p,U), \tag{26}$$

$$b(\rho,\xi) = \int_{-\infty}^{+\infty} d\kappa \frac{\sin\kappa}{\kappa^2} e^{i\kappa\rho} e^{i\xi\sqrt{1+(\kappa/p)^2}(1-\kappa U)}, \tag{27}$$

with $\kappa = k_\perp a/2$, and the self-consistent, parallel current density takes the form

$$j_z(y,z;\omega) = \frac{\sigma_0\omega}{2\pi} j_s(\rho,\xi;p,U), \tag{28}$$

$$j_s(\rho,\xi) = \int_{-\infty}^{+\infty} d\kappa \frac{\sin\kappa}{\kappa} e^{i\kappa\rho} e^{i\xi\sqrt{1+(\kappa/p)^2}(1-\kappa U)}. \tag{29}$$

In the absence of plasma flow ($U=0$), Eq. (27) corresponds to the slab version of the magnetic field structure investigated in Ref. 10, hence no detailed analysis is presented here. In general, the magnetic field structure (for $U=0$) is essentially that generated by a current channel whose boundary expands in the (y, z) plane along the cone angle given by Eq. (10). For slab geometry, this implies that near the axis ($|y| \ll a/2$) $B_y \propto y$, while outside the cone angle $|B_y|$ attains a constant value, but with the direction of B_y determined by the usual right-hand rule. This perspective on the effect of electron inertia in the expansion of a current channel is useful in interpreting the numerical results presented later.

For large current channels (i.e., $p \to \infty$), the effect of electron inertia is negligible and Eq. (29) reduces to

$$j_s \to \int_{-\infty}^{+\infty} d\kappa \frac{\sin\kappa}{\kappa} e^{i\kappa(\rho - U\xi)}, \tag{30}$$

which indicates that the current channel is rigidly convected by the flow along the trajectory $\rho = U\xi$. This implies that the center of the channel follows the angle given by Eq. (12), i.e., the ideal MHD result.

The nontrivial interplay between the forcing effect of the flow and the bounded expansion associated with electron inertia can be illustrated by considering the behavior of j_s in the asymptotic limit of large ξ. As can be deduced from the exponent proportional to ξ in the integrand of Eq. (29), as ξ increases the significant contributions to the integral arise from values of κ/p that are not too large, hence the major features of the current channel are contained in the approximate form

$$j_s \sim \int_{-\infty}^{+\infty} d\kappa\, e^{i\kappa\rho} e^{i\xi[1+(1/2)(\kappa/p)^2](1-\kappa U)}, \tag{31}$$

in which the square root is approximated by the lowest order quadratic (in κ) term, and $\sin\kappa/\kappa \to 1$, also to lowest order in κ.

The integrand in Eq. (31) consists of a pure phase factor which is a third-order polynomial in terms of the variable of integration κ. It is thus possible to add and subtract terms to complete the closed-form expression for a cubic of the type $(\alpha+\beta\kappa)^3$ and to deduce the values of α and β. Furthermore, by suitable rescaling the resulting integral can be identified with the familiar expression[18] for the Airy function Ai. Performing the straightforward steps results in the expression

$$j_s \sim \frac{2\pi}{\Delta} e^{i(\xi+\psi)} Ai\left(\frac{-r}{\Delta}\right), \tag{32}$$

where

$$r = (\rho - U\xi) + \frac{\xi}{6Up^2}, \tag{33}$$

$$\Delta = \left(\frac{3\xi U}{2p^2}\right)^{1/3}, \tag{34}$$

$$\psi = \frac{1}{3U}\left[\rho - \left(U - \frac{1}{9Up^2}\right)\xi\right]. \tag{35}$$

Recalling that the function Ai is evanescent for positive argument and has its maximum value where the argument is close to zero helps to identify the physical meaning of the quantity r. The peak of the current channel follows a trajectory in the (y, z) plane given approximately by $r=0$. From Eq. (33), it is seen that to leading order the trajectory corresponds to the ideal MHD prediction of Eq. (12), but has a correction associated with the combined effect of flow and electron inertia which scales as Up^2.

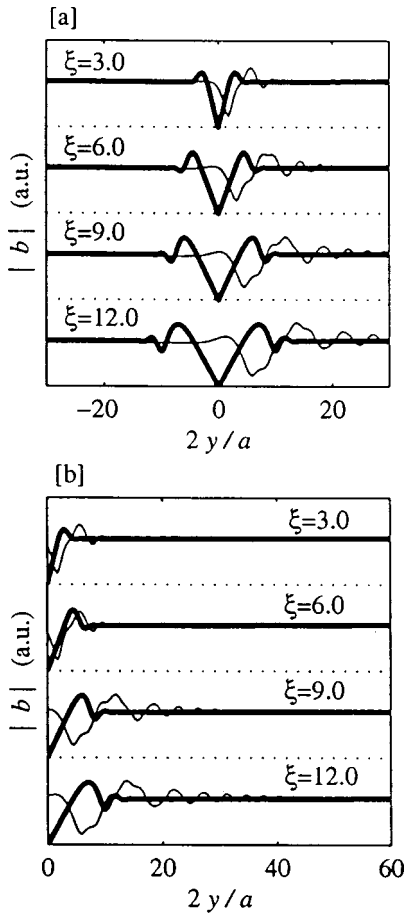

FIG. 3. Transverse spatial dependence of magnitude of scaled magnetic field for different axial positions. Heavier curves are in the absence of flow, and lighter curves when $U=0.5$. (b) is the same as (a) but over an expanded transverse distance. $p=1.0$. Dotted line is zero baseline for curves immediately above.

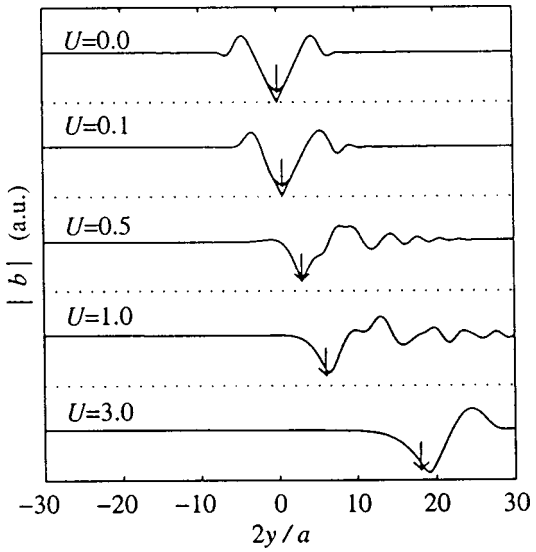

FIG. 4. Effect of increasing scaled drift-velocity on transverse spatial dependence of magnitude of scaled magnetic field at fixed scaled axial position $\xi=6.0$; $p=1.0$. Arrow indicates location of center of current channel predicted by ideal MHD. Dotted lines are zero baseline for curves immediately above.

Since the Ai function oscillates for negative argument, this implies that the initial, unipolar current channel breaks up into an array of adjacent current filaments having opposite polarity. As y increases, the transverse extent of the filaments becomes narrower, however, the first lobe near $r=0$ has a width determined by the quantity Δ given by Eq. (34). The motion of the oscillatory current channel in the (y, z) plane in turn introduces an additional phase to the self-consistent shear Alfvén wave, and is represented by the quantity ψ in Eq. (35).

IV. SPATIAL PATTERN

To illustrate the modifications produced by plasma flow on the spatial pattern of a small-scale shear Alfvén wave, the integrals given by Eqs. (27) and (29) are evaluated numerically. Because the phenomena is determined by sensitive phase-mixing terms and in order to properly resolve the oscillatory terms in the various regions, the width of the interval summed over in the numerical integration was chosen by incrementally decreasing it until the numerical value of the integral was unchanged within machine precision.

Figure 3 displays the transverse spatial dependence of the magnitude of the scaled magnetic field, $|b|$, for different axial positions away from the exciter whose dimension is $a=2c/\omega_{pe}$ (i.e., $p=1.0$). The heavier curves correspond to zero flow while the lighter curves are in the presence of a scaled drift $2v_D/(a\omega)=0.5$. Panel (b) uses an expanded scale along the positive y direction to display the extended pattern that is generated by the flowing plasma. The dotted lines in Fig. 3 represent the zero baseline for the curves immediately above them. It is seen from Fig. 3 that in the absence of plasma flow the magnetic field associated with the axial current spreads symmetrically about $y=0$ according to the cone angle given by Eq. (10). The constant level achieved by $|b|$ at larger values of y indicates that the axial current channel is confined within the cones. Since the current channel spreads as ξ increases, the slope of $|b|$ at $y=0$ becomes progressively smaller. The behavior displayed by the lighter curves in Fig. 3 illustrates that the plasma flow convects the magnetic field in the direction of the flow, and in addition it gives rise to oscillations in the magnitude of $|b|$, i.e., partially standing waves are generated across the confining magnetic field, as expected from the discussion in Sec. II associated with Fig. 1. Of course, oscillations in the magnitude of B_x imply reversals in the direction of the axial current density.

The effect of increasing drift velocity on the transverse variation of the magnitude of the scaled magnetic field, $|b|$, at a fixed axial position $\xi=6.0$ is shown in Fig. 4 for $p=1.0$. The arrows in Fig. 4 correspond to the position of the center of the current channel predicted by ideal MHD. It is seen from Fig. 4 that as U increases the overshoot on the left-side normally associated with the counter-propagating cone is smoothed out, while on the right-hand side the edge of the co-moving cone breaks up into an increasing number of oscillations.

Since the value of the local magnetic field is determined by contributions due to the current density over large dis-

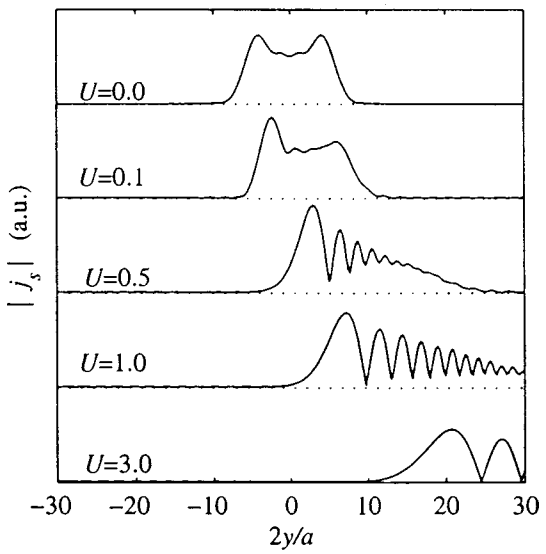

FIG. 5. Transverse spatial dependence of the magnitude of the scaled axial current density for different scaled flow speeds U at a fixed axial position $\xi=6.0$; $p=1.0$.

tances, it is not readily evident from Figs. 3 and 4 what the distortions induced on the initial flat-top current channel by the plasma flow are. To clearly illustrate the changes, Fig. 5 displays the transverse spatial pattern of the magnitude of the scaled axial current density $|j_s|$ at a fixed axial position $\xi=6.0$, for different flow speeds, obtained directly from Eq. (29). Figure 5 documents a continuous transition from the spreading pattern resulting from the collisionless electron skin-depth ($U=0.0$), first into a convected current channel exhibiting minor distortions ($U=0.1$), and which evolves at $U=1.0$ into an Airy-like structure, as suggested by the results leading to Eq. (32). Clearly, the behavior exhibited for $U\geqslant 1.0$ is very different from the prediction of ideal MHD, and looks so different from the initial flat-top that it would be difficult for someone making a laboratory measurement or an observation onboard a spacecraft to establish a causal relationship between the two.

V. CONCLUSIONS

This analytic study illustrates a subtle feature resulting from the interplay between a cross-field, bulk plasma flow and finite electron inertia in the evolution of Alfvénic current channels whose transverse scale is on the order of the electron skin-depth. It is found that an initial flat-top current channel evolves into an array of adjacent current filaments of opposite polarity and decreasing spatial extent. The transition to this unusual pattern occurs for drift-velocities that satisfy the condition $v_D\approx(\omega/\omega_{pe})c$, where c is the speed of light and ω is the frequency ($\omega\ll\Omega_i$) at which the current is modulated.

Since the current filamentation process illustrated here is strictly a linear interaction, it may have consequences for the interpretation of laboratory measurements and spacecraft observations, because phenomena of this type are typically associated with nonlinear coupling. Of course, in the description of Alfvénic turbulence, distortions of the type described here are naturally present and can result in unusual structures.

Finally, since shear Alfvén waves are highly collimated, the type of distortions illustrated in the present study could be used, under appropriate conditions, as a diagnostic tool to probe regions where interesting plasma flows are present.

ACKNOWLEDGMENT

This work is sponsored by the Office of Naval Research.

[1] S. DeSouza-Machado, A. B. Hassam, and R. Sina, Phys. Plasmas **7**, 4632 (2000).
[2] Y. Idomura, M. Wakatani, and S. Tokuda, Phys. Plasmas **7**, 3551 (2000).
[3] R. E. Waltz, R. L. Dewar, and X. Garbet, Phys. Plasmas **5**, 1784 (1998).
[4] H. Biglari, P. H. Diamond, and P. W. Terry, Phys. Fluids B **2**, 1 (1990).
[5] P. S. Joarder and S. Narayan, Astron. Astrophys. **359**, 1211 (2000).
[6] J. I. Sakai, T. Kawata, K. Yoshida, K. Furusawa, and N. F. Cramer, Astrophys. J. **537**, 1063 (2000).
[7] J. R. Peñano and G. Ganguli, J. Geophys. Res. **105**, 7441 (2000).
[8] G. Ganguli, Y. C. Lee, and P. J. Palmadesso, Phys. Plasmas **31**, 823 (1988).
[9] G. D. Earle, M. C. Kelley, and G. Ganguli, J. Geophys. Res. **94**, 15321 (1984).
[10] G. Ganguli, M. J. Keskinen, H. Romero, R. Heelis, T. Moore, and C. Pollock, J. Geophys. Res. **99**, 8873 (1994).
[11] T. E. Moore, M. O. Chandler, C. J. Pollock, D. L. Reasoner, R. L. Arnoldy, B. Austin, P. M. Kintner, and J. Bonnell, J. Geophys. Res. **101**, 5279 (1996).
[12] F. Wagner, G. Becker, K. Behringer *et al.*, Phys. Rev. Lett. **49**, 1408 (1982).
[13] R. J. Taylor, M. L. Brown, B. D. Fried, H. Grote, J. R. Liberati, G. J. Morales, P. Prybil, D. Darrow, and M. Ono, Phys. Rev. Lett. **63**, 2365 (1989).
[14] G. J. Morales, R. S. Loritsch, and J. E. Maggs, Phys. Plasmas **1**, 3765 (1994).
[15] P. M. Bellan, Phys. Plasmas **1**, 3523 (1994).
[16] W. Gekelman, D. Leneman, J. Maggs, and S. Vincena, Phys. Plasmas **1**, 3775 (1994).
[17] D. Leneman, W. Gekelman, and J. Maggs, Phys. Plasmas **7**, 3934 (2000).
[18] H. A. Antosiewicz, *Handbook of Mathematical Functions*, 9th ed., edited by M. Abramowitz and I. A. Stegun (Dover, New York, 1972), p. 447.